RSC Advances

Check for updates

Prediction of pressure-induced phase transformations in Mg₃As₂†

Kang Yang, Jingming Shi, [ID] * Shicong Ding, Ruiming Su, Wenwen Cui, Meiling Xu, [ID] Jian Hao* and Yinwei Li

Pressure is a fundamental tool that can induce structural and electronic transformations, which is helpful to search for exotic materials not accessible at ambient conditions. Here, we have performed an extensive structural study on cubic Mg_3As_2 in a pressure range of 0–100 GPa by using a combination of structure predictions and first-principle calculations. Interestingly, two novel structures with space groups $C2/m$ and $P\bar{1}$ were uncovered that become energetically most stable at pressures of 12 GPa and 30 GPa, respectively. Phonon dispersions demonstrate that the three phases are dynamically stable in their respective low-enthalpy pressure ranges. The electronic calculations show that Mg_3As_2 keeps semiconductor properties at pressures up to 100 GPa. The interesting thing is that the direct semi-conducting property of Mg_3As_2 transforms into indirect semi-conducting when the pressure is above 12 GPa. The current results provide new insights for understanding the behavior of Mg_3As_2 at high pressures.

1 Introduction

Pressure is considered as one of the most fundamental thermodynamic variables which can be used to influence the structural configuration, electronic properties and synthesis of unusual stoichiometric materials.[1–9] These fruitful results indicate that pressure is a powerful tool for discovering and designing novel materials which possess unique properties, like being super conductive, super hard, and transparent semiconductive.

Group II alkaline metal elements typically form A_3B_2-type compounds with the elements in group V. These compounds have attracted much attention due to their wide band gaps and can be viewed as good materials in electronic and optoelectronic devices. Mg_3N_2, a typical A_3B_2-type compound, has been identified to crystallize in the cubic anti-bixbyite structure of the mineral $(Mn,Fe)_2O_3$ (ref. 10) with space group $Ia\bar{3}$ at ambient conditions. Experimental studies have shown that the cubic Mg_3N_2 undergoes several phase transformations[11,12] to $C2/m$[13] and $P\bar{3}m1$ (ref. 13) at high pressure. While for another compound in this group, Ca_3N_2, numerous phases have been synthesized at the experimental level or predicted in theoretical simulations, namely $Ia\bar{3}$,[14,15] $R\bar{3}c$,[16,17] $Pbcn$,[18] $C2/m$,[19] $P\bar{3}m1$,[19] and $I\bar{4}3d$.[20] In 2017, a phase transition of Mg_3P_2 was found by theoretical simulation when going from ambient conditions to high pressure.[21] It reveals that there are four

phases of Mg_3P_2 in the A_3B_2-type family that are stable in the pressure range from the ambient to 100 GPa. The previous studies have shown that most of the structures of the A_3B_2-type family possess $Ia\bar{3}$ symmetry which is the typical configuration of rare-earth sesquioxides (e.g., Sc_2O_3,[22] Y_2O_3,[23] Er_2O_3,[24] Gd_2O_3,[25] In_2O_3 (ref. 26)). As, the sister element to N and P elements in group VA, exhibits the similar electron-cloud out of the core and possesses similar chemical properties. In early 1964, Juza and Kroebel experimentally found two phases of Mg_3As_2, namely $Ia\bar{3}$ and $P\bar{3}m1$,[27] which were also reported by Ali Mokhtari and Matin Sedighi in 2010 with simulation[28] and collected by the Materials Project database.[29] However, the As atom has a much larger ionic radius than N and P atoms, which may affect the structural configuration of arsenide and the phase transformation sequence, especially at high pressure. On the other hand, the existent compounds of the A_3B_2-type family usually have large band gaps, which is beneficial to potential applications. For example, the band gap of Mg_3N_2 (ref. 13) is about 1.65 eV at ambient conditions and 2.35 eV at about 25 GPa, respectively. While for the Mg_3P_2 compound,[21] the gap is about 1.73 eV and 1.14 eV at ambient conditions and 2.5 GPa, respectively. When the pressure is above 35 GPa, Mg_3P_2 transforms into a metallic phase. Thus, there is a lot of necessity for us to study the band gap evolution and the potential applications of Mg_3As_2 from ambient conditions to high pressure. Finally, as an antistructure in comparison to the traditional A_2B_3-type, accurate structural configuration and the phase transition sequence of Mg_3As_2 under high pressure can provide important implications for understanding the compressional behavior of related materials like rare-earth sesquioxides.

School of Physics and Electronic Engineering, Jiangsu Normal University, Xuzhou, China. E-mail: jingmingshi@jsnu.edu.cn; jian_hao@jsnu.edu.cn

In order to clarify the phase transitions and potential electronic applications of Mg_3As_2 compounds from ambient conditions to high pressure, we performed systematic structural searches by using a structural prediction method combining with the first-principles method. We predicted two novel structures of Mg_3As_2 that are unknown in the pressure range from ambient to 100 GPa. The phonon dispersions show that all the novel phases of Mg_3As_2 were dynamically stable. Electronic property calculations show that all the phases of Mg_3As_2 can be viewed as semiconductors. Interestingly, with the pressure increasing, the character of direct semiconductor (for $P\bar{3}m1$ and $C2/m$ phases) will turn into an indirect band gap property ($P\bar{1}$ phase).

2 Methods

For the structure stability, we used two steps to get the ground state structure at each pressure. Firstly, as the elements with similar electron clouds always form the same structure configuration, we chose the known phases of Mg–N and Mg–P (like $Ia\bar{3}$, $C2/m$ and $P\bar{3}m1$) as prototype structures to predict the novel phase of the Mg–As system. Secondly, we performed structure predictions to search all the possible structures in the energy surface. For the structure prediction we used the CALYPSO[30,31] method with the cells containing 2 to 4 formula units in a pressure range from 0 to 100 GPa. The underlying *ab initio* structural relaxations and the electronic band structure calculations were performed in the framework of density functional theory (DFT) using the VASP code.[32] The calculations were carried out in the generalized gradient approximation[33] for the exchange–correlation potential, using the Perdew–Burke–Ernzerhof[34] (PBE) functional. The electronic wave functions were expanded in a plane wave basis set with a cutoff energy of 600 eV. The electron–ion interaction was described by means of projector augmented wave (PAW)[35] pseudopotentials with $2p^63s^2$ and $3s^23p^3$ electrons in the valence band for the Mg and As atoms, respectively. Monkhorst–Pack k-point[36] meshes with a grid density of 0.03 $\mathring{A}^{-1}$ were chosen to achieve a total energy convergence of better than 1 meV per atom. The phonon dispersion curves were computed by the direct supercell calculation method, as implemented in the PHONOPY program.[37]

3 Results and discussions

To investigate the phase transitions of Mg_3As_2, we performed structural prediction with unit-cell sizes of maximal four formula units (f.u.) at pressures of 0, 20, 50 and 100 GPa, respectively. Due to computational restrictions, we decided to use a suitable unit-cell size to ensure the calculation efficiency. For the next step, we chose at least 5 structures in each prediction for further accurate geometric optimization. The phase transitions of Mg_3As_2 under high pressure are further illustrated in Fig. 1, where we plot the relative enthalpies per formula unit with respect to the $C2/m$ phase as a function of pressure, including the enthalpies of metastable phases that we predicted. From Fig. 1, we can clearly find that the $Ia\bar{3}$ phase is
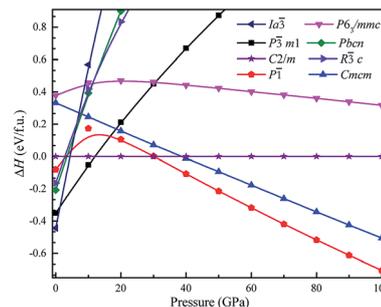

Fig. 1 Relative enthalpy per formula unit of the different phases of Mg_3As_2 with respect to the $C2/m$ phase as a function of pressure.

the ground-state for Mg_3As_2 at ambient conditions. The crystal structure of this phase is shown in Fig. 2(a). The $Ia\bar{3}$ phase has an interesting configuration with Mg–As bond lengths of 2.62–2.73 Å. There are eight formula units in its primitive cell and all the Mg atoms are in the same Wyckoff positions (48e) while two different As atoms possess the (8b) and (24d) positions. In this phase, each Mg atom connects with four As atoms, while each As atom is bonded to six Mg atoms. However, the $Ia\bar{3}$ phase is quickly destabilized by pressure, and a novel structure with space group $P\bar{3}m1$ becomes the ground-state at a pressure of 1.3 GPa. The crystal configuration of this phase is shown in Fig. 2(b). This phenomenon also emerges in the similar system of Mg_3P_2.[21] The $P\bar{3}m1$ phase has five atoms in its primitive cell. The Mg atoms possess Wyckoff positions of (2d) and (1a), while the As atoms only locate at (2d) positions. The Mg atoms and As atoms form an octahedron and tetrahedron with Mg–As bond lengths of 2.62–2.73 Å. These behaviors are in good agreement with the information that was presented in the Materials Project
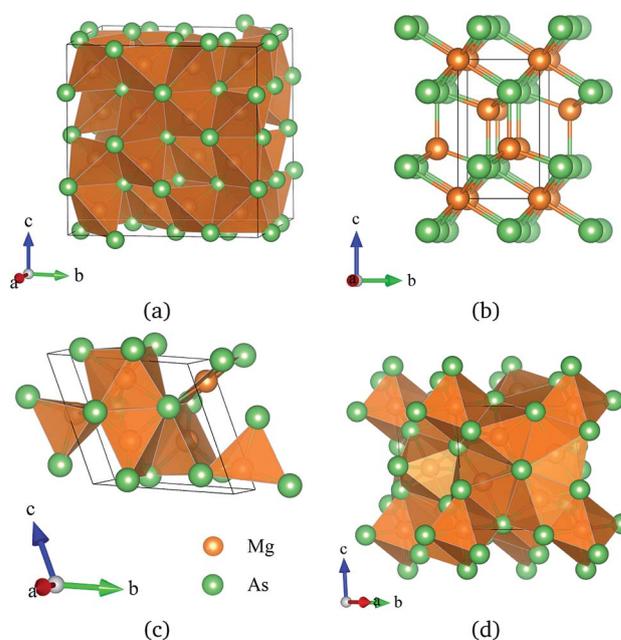

Fig. 2 Crystal structures of Mg_3As_2 (orange: Mg and green: As); (a) the $Ia\bar{3}$ phase at ambient pressure, (b) the $P\bar{3}m1$ phase at 5 GPa, (c) the $C2/m$ phase at 15 GPa and (d) the $P\bar{1}$ phase at 30 GPa.

database.[29] When the pressure increases, the $C2/m$ phase becomes energetically favorable at around 12 GPa. The $C2/m$ structure has two formula units in its unit cell, as shown in Fig. 2(c). This is a remarkable structure which is composed of a regular octahedron and a tetrahedron. They connect to each other with a sharing edge formed by two As atoms. The distances between the Mg atom and As atom are 2.47–2.73 Å at 20 GPa. With the pressure increasing to 30 GPa, we predict a novel phase with $P\bar{1}$ symmetry which is energetically favored in a large range of pressures from about 30 GPa to more than 100 GPa, the maximum pressure we considered. The $P\bar{1}$ phase has an interesting structural configuration with several octahedrons and they connect with each other by sharing one or two faces, as shown in Fig. 2(d). The distances between the Mg and As atoms are around 2.50–2.65 Å under 30 GPa. Thus, we propose a clear phase transformation sequence of Mg_3As_2 from ambient conditions to high pressure. The sequence is as follows: $Ia\bar{3} \xrightarrow{1.3 \text{ GPa}} P\bar{3}m1 \xrightarrow{12 \text{ GPa}} C2/m \xrightarrow{30 \text{ GPa}} P\bar{1}$. Comparing with the series of phase transitions of Mg_3N_2 ($Ia\bar{3} \xrightarrow{20.6 \text{ GPa}} C2/m \xrightarrow{67 \text{ GPa}} P\bar{3}m1$)[13] and Mg_3P_2 ($Ia\bar{3} \xrightarrow{2.5 \text{ GPa}} P\bar{3}m1 \xrightarrow{35 \text{ GPa}} P6_3/mmc \xrightarrow{65 \text{ GPa}} C2/c$),[21] we can find that these three compounds adopt the same ambient structure, while high pressure phases vary accordingly, which is caused by the different ionic radii of N, P and As atoms. The lattice parameters and atomic coordinates which are optimized for the most energetically favorable structures are listed in Table 1. The lattice parameters of $Ia\bar{3}$ ($a = 12.16$ Å) are in good agreement with the data in the Materials Project ($a = 12.176$ Å),[29] which indicates that our calculations are credible. To examine the interactions between Mg and As atoms of the new

phases, we calculated the Bader charges, as shown in Table 1. The results show that all the phases of Mg_3As_2 compound exhibit ionic behavior and each Mg atom will lose about $1.50e$ while each As atom will gain about $2.25e$. To understand the bonding behaviors of these structures, we calculated the electron localization function (ELF) and the charge density difference, as shown in the ESI.† The results show that the charges almost localize around the As atoms that form anions, while Mg atoms act as cations. This is also in good agreement with the results of the Bader analysis.

We also calculated the lattice parameters and volumes of these four novel phases of Mg_3As_2 as a function of pressure, as shown in Fig. 3. It reveals that all the lattice constants will decrease when the pressure increases and detects that the volume collapses at the phase transitions: $Ia\bar{3} \rightarrow P\bar{3}m1$ (at 1.3 GPa), $P\bar{3}m1 \rightarrow C2/m$ (at 12 GPa) and $C2/m \rightarrow P\bar{1}$ (at 30 GPa). This indicates that the three phase transitions in Mg_3As_2 are first-order in nature. This phenomenon is in good agreement with the previous works on Mg_3P_2.[21]

In order to ensure the thermal stability of these novel structures, we calculated the phonon dispersions of $Ia\bar{3}$, $P\bar{3}m1$, $C2/m$ and $P\bar{1}$ at 0, 1.5, 20 and 30 GPa, respectively, as shown in Fig. 4. As expected, they do not exhibit any imaginary phonon frequencies indicating that all the novel phases are mechanically stable. It is well known that the PBE function systematically underestimates band gaps. Therefore we decided to adopt the hybrid exchange–correlation functional of Heyd, Scuseria, and Ernzerhof (HSE06)[38] to obtain reliable band gaps. The calculated electronic band structures (HSE06) and the projected densities of state (HSE06) are shown in Fig. 5. For comparison,

Table 1 Predicted crystal structures of Mg_3As_2 in its $Ia\bar{3}$, $P\bar{3}m1$, $C2/m$ and $P\bar{1}$ phases at selected pressures. Bader charges of these phases at specific conditions are shown in the last column

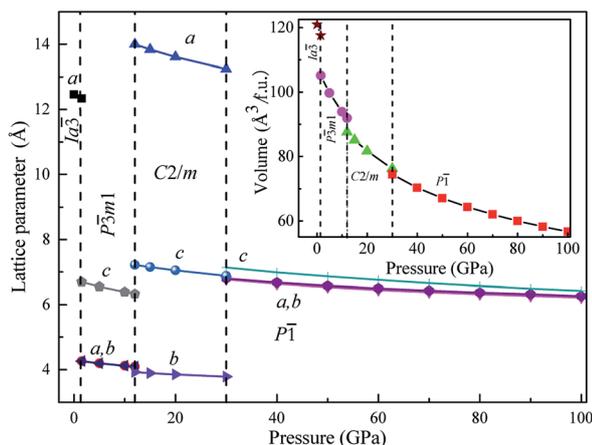| Pressure (GPa)	Space group	Lattice parameters	Atomic coordinates (fractional)	Bader charge (e)
0	$Ia\bar{3}$	$a = b = c = 12.46$ Å	Mg (48e) (−0.11, −0.36, 0.88)	1.51
		$\alpha = \beta = \gamma = 90°$	As (8b) (−0.25, −0.25, 0.75)	−2.26
			As (24d) (−0.02, −1.00, 0.25)	−2.26
5	$P\bar{3}m1$	$a = b = 4.19$ Å	Mg (2d) (0.33, 0.67, 0.36)	1.50
		$c = 6.55$ Å	Mg (1a) (0.00, 0.00, 0.00)	1.56
		$\alpha = \beta = 90°, \gamma = 120°$	As (2d) (0.33, 0.67, 0.77)	−2.28
15	$C2/m$	$a = 13.84$ Å	Mg (4i) (0.34, 0.50, 0.02)	1.49
		$b = 3.89$ Å	Mg (4i) (0.25, 0.00, 0.66)	1.52
		$c = 7.15$ Å	Mg (2c) (0.50, 0.50, 0.50)	1.55
		$\alpha = 116.67°$	Mg (2b) (0.50, 0.00, 1.00)	1.53
		$\beta = 105.80°$	As (4i) (0.13, 0.50, 0.74)	−2.29
		$\gamma = 90°$	As (4i) (0.40, 0.50, 0.73)	−2.26
30	$P\bar{1}$	$a = 6.77$ Å	Mg (2i) (0.52, 0.53, 0.72)	1.56
		$b = 6.80$ Å	Mg (2i) (0.23, 0.23, 0.15)	1.56
		$c = 7.14$ Å	Mg (2i) (0.09, 0.77, 0.61)	1.54
		$\alpha = 93.32°$	Mg (2i) (0.97, 0.67, 0.25)	1.55
		$\beta = 97.04°$	Mg (2i) (0.50, 0.79, 0.110)	1.55
		$\gamma = 65.85°$	Mg (1a) (0.00, 0.00, 0.00)	1.54
			Mg (1f) (0.50, 0.00, 0.50)	1.58
			As (2i) (0.33, 0.95, 0.80)	−2.35
			As (2i) (0.21, 0.89, 0.32)	−2.31
			As (2i) (0.79, 0.43, 0.04)	−2.37
			As (2i) (0.75, 0.61, 0.51)	−2.26

Fig. 3 Lattice parameters and volume of Mg_3As_2 as a function of pressure.

the calculated band structures of all structures by using the PBE function are shown in the ESI.† From our calculation, it is evident that all the four phases of Mg_3As_2 are semiconductors and the band gap will decrease with increasing pressure. For example, at 0 GPa, the band gap of the $Ia\bar{3}$ phase is 1.42 eV (PBE) and 2.08 eV (HSE06), which is in good agreement with the previous work,[28] while it will become 0.86 eV (PBE) and 1.43 eV (HSE06) for $P\bar{3}m1$ at 1.5 GPa, 0.68 eV (PBE) and 1.21 eV (HSE06) for $C2/m$ at 20 GPa and 0.49 eV (PBE) and 0.93 eV (HSE06) for $P\bar{1}$ at 30 GPa, respectively. Comparing to another two compounds (Mg_3N_2 (ref. 13) and Mg_3P_2 (ref. 21)), Mg_3As_2 has a larger band gap at ambient conditions and can remain a semiconductor even at high pressure. These good performances can make Mg_3As_2 compounds act as good potential semiconductors at both ambient conditions and high pressure. The projected densities of state show that the electrons near the Fermi level are almost all contributed by the As atoms, which reveals that the As atoms play an important role in the semiconductor property.
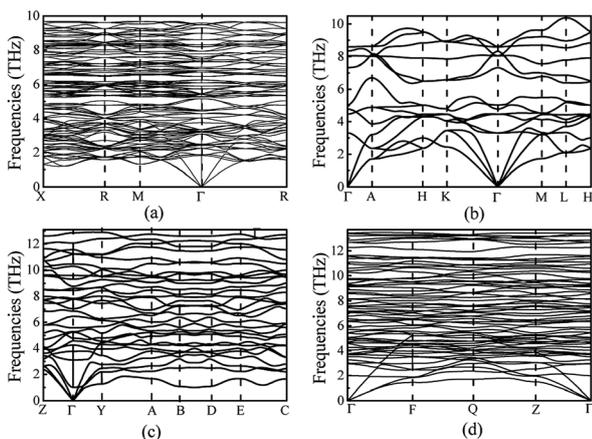
Fig. 5 Electronic band structures and densities of state (HSE06) of Mg_3As_2 for (a) the $Ia\bar{3}$ phase at ambient pressure, (b) the $P\bar{3}m1$ phase at 1.5 GPa, (c) the $C2/m$ phase at 20 GPa and (d) the $P\bar{1}$ phase at 30 GPa.
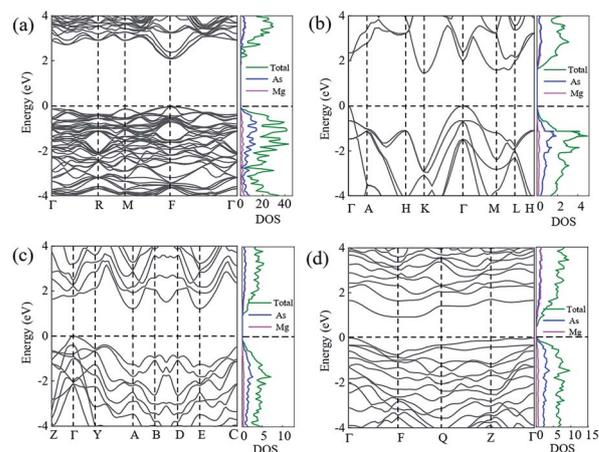
4 Conclusions

In summary, using a global structural prediction method we studied systematically the phase transitions and electronic properties of Mg_3As_2. We identified two novel phases with unexpected structures that might be experimentally synthesizable over a wide range of pressures. The novel phases have $C2/m$ and $P\bar{1}$ symmetry under high pressure. The transition pressures of the two structures are 12 GPa and 30 GPa, respectively. The Bader charge calculations show that all the phases possess ionic behavior. The phonon dispersions reveal that they are mechanically stable. From the calculations of electronic properties we can indicate that all the phases are semiconductor. These results show remarkable phase transitions of Mg_3As_2, and can serve as an important guide for further experimental studies of this compound.

Conflicts of interest

There are no conflicts to declare.

Acknowledgements

Fig. 4 Phonon dispersions of Mg_3As_2 for (a) the $Ia\bar{3}$ phase at ambient pressure, (b) the $P\bar{3}m1$ phase at 1.5 GPa, (c) the $C2/m$ phase at 20 GPa and (d) the $P\bar{1}$ phase at 30 GPa.

References

1 L. Zhang, Y. Wang, J. Lv and Y. Ma, *Nat. Rev. Mater.*, 2017, **2**, 17005.

2 Y. Ma, M. Eremets, A. R. Oganov, Y. Xie, I. Trojan, S. Medvedev, A. O. Lyakhov, M. Valle and V. Prakapenka, *Nature*, 2009, **458**, 182–185.

3 Y. Li, Y. Wang, C. J. Pickard, R. J. Needs, Y. Wang and Y. Ma, *Phys. Rev. Lett.*, 2015, **114**, 125501.

4 Y. Li, J. Hao, H. Liu, Y. Li and Y. Ma, *J. Chem. Phys.*, 2014, **140**, 899.

5 A. Drozdov, M. Eremets, I. Troyan, V. Ksenofontov and S. Shylin, *Nature*, 2015, **525**, 73.

6 D. Duan, Y. Liu, F. Tian, D. Li, X. Huang, Z. Zhao, H. Yu, B. Liu, W. Tian and T. Cui, *Sci. Rep.*, 2014, **4**, 6968.

7 Y. Li, X. Feng, H. Liu, J. Hao, S. A. Redfern, W. Lei, D. Liu and Y. Ma, *Nat. Commun.*, 2018, **9**, 722.

8 Y. Li, J. Hao, H. Liu, S. Lu and J. S. Tse, *Phys. Rev. Lett.*, 2015, **115**, 105502.

9 J. Shi, W. Cui, S. Botti and M. A. L. Marques, *Phys. Rev. Mater.*, 2018, **2**, 023604.

10 M. Stackelberg and R. Paulus, *Z. Phys. Chem. B*, 1933, **22**, 305–322.

11 D. Partin, D. Williams and M. O'Keeffe, *J. Solid State Chem.*, 1997, **132**, 56–59.

12 F. Zong, C. Meng, Z. Guo, F. Ji, H. Xiao, X. Zhang, J. Ma and H. Ma, *J. Alloys Compd.*, 2010, **508**, 172–176.

13 J. Hao, Y. Li, Q. Zhou, D. Liu, M. Li, F. Li, W. Lei, X. Chen, Y. Ma, Q. Cui, *et al.*, *Inorg. Chem.*, 2009, **48**, 9737–9741.

14 H. Moissan, *Compt. Rend.*, 1898, **127**, 497–501.

15 O. Reckeweg and F. J. DiSalvo, *Z. Anorg. Allg. Chem.*, 2001, **627**, 371–377.

16 H. H. Franck, M. A. Bredig and G. Hoffmann, *Naturwissenschaften*, 1933, **21**, 330–331.

17 H. Hartmann and H. J. Fröhlich, *Z. Anorg. Allg. Chem.*, 1934, **218**, 190–192.

18 R. S. Bradley, D. C. Munro and M. Whitfield, *J. Inorg. Nucl. Chem.*, 1966, **28**, 1803–1812.

19 J. Hao, Y. Li, J. Wang, C. Ma, L. Huang, R. Liu, Q. Cui, G. Zou, J. Liu and X. Li, *J. Phys. Chem. C*, 2010, **114**, 16750–16755.

20 C. Braun, S. L. Börger, T. D. Boyko, G. Miehe, H. Ehrenberg, P. Höhn, A. Moewes and W. Schnick, *J. Am. Chem. Soc.*, 2011, **133**, 4307.

21 B. Liu, J. Hao, X. Tang and Y. Li, *J. Alloys Compd.*, 2017, **720**, 207–211.

22 T. Schleid and G. Meyer, *J. Less-Common Met.*, 1989, **149**, 73–80.

23 B. Antic, P. Oennerud, D. Rodic and R. Tellgren, *Powder Diffr.*, 1993, **8**, 216–220.

24 Q. Guo, Y. Zhao, C. Jiang, W. L. Mao, Z. Wang, J. Zhang and Y. Wang, *Inorg. Chem.*, 2007, **46**, 6164–6169.

25 F. Zhang, M. Lang, J. Wang, U. Becker and R. Ewing, *Phys. Rev. B: Condens. Matter Mater. Phys.*, 2008, **78**, 064114.

26 H. Yusa, T. Tsuchiya, J. Tsuchiya, N. Sata and Y. Ohishi, *Phys. Rev. B: Condens. Matter Mater. Phys.*, 2008, **78**, 092107.

27 R. Juza and R. Kroebel, *Z. Anorg. Allg. Chem.*, 1964, **331**, 187–199.

28 A. Mokhtari and M. Sedighi, *Phys. Rev. B: Condens. Matter Mater. Phys.*, 2010, **405**, 1715–1720.

29 A. Jain, S. P. Ong, G. Hautier, W. Chen, W. D. Richards, S. Dacek, S. Cholia, D. Gunter, D. Skinner, G. Ceder, *et al.*, *APL Mater.*, 2013, **1**, 011002.

30 Y. Wang, J. Lv, L. Zhu and Y. Ma, *Phys. Rev. B: Condens. Matter Mater. Phys.*, 2010, **82**, 094116.

31 Y. Wang, J. Lv, L. Zhu and Y. Ma, *Comput. Phys. Commun.*, 2012, **183**, 2063–2070.

32 G. Kresse and J. Hafner, *Phys. Rev. B: Condens. Matter Mater. Phys.*, 1993, **47**, 558.

33 G. Kresse and D. Joubert, *Phys. Rev. B: Condens. Matter Mater. Phys.*, 1999, **59**, 1758.

34 J. P. Perdew, K. Burke and M. Ernzerhof, *Phys. Rev. Lett.*, 1996, **77**, 3865.

35 G. Kresse and D. Joubert, *Phys. Rev. B: Condens. Matter Mater. Phys.*, 1999, **59**, 1758.

36 H. J. Monkhorst and J. D. Pack, *Phys. Rev. B: Solid State*, 1976, **13**, 5188.

37 A. Togo, F. Oba and I. Tanaka, *Phys. Rev. B: Condens. Matter Mater. Phys.*, 2008, **78**, 134106.

38 J. Heyd, G. E. Scuseria and M. Ernzerhof, *J. Chem. Phys.*, 2003, **118**, 8207–8215.

39 K. Momma and F. Izumi, *J. Appl. Crystallogr.*, 2011, **44**, 1272–1276.